Additive Manufacturing 85 (2024) 104163

Contents lists available at ScienceDirect

Additive Manufacturing

journal homepage: www.elsevier.com/locate/addma

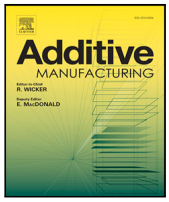

Research paper

A shape-predictive model for the spreading of photo-curable polymers in material extrusion additive manufacturing

Amir Azimi Yancheshme, Heedong Yoon, Giuseppe R. Palmese, Nicolas J. Alvarez *

Chemical and Biological Engineering, Drexel University, Philadelphia, PA 19104, USA

ARTICLE INFO

Keywords:
Material extrusion
Photopolymerization
Bead spreading
Shape-predictive model

ABSTRACT

Recently, there is a growing interest in material extrusion to print thermoset resins to manufacture large format and high-performance parts. However, the fidelity and mechanical integrity of the printed parts are limited by challenges such as uncontrolled spreading of individual beads (filament/droplet) after deposition and during cure. There is a considerable lack of experimental and theoretical studies on the spreading of reactive beads on solid substrates. In this work, we studied the simultaneous spreading and photo-curing of the photopolymerizable thermoset beads via experiment and numerical simulations. We used a novel experimental setup to track the spreading of droplets and filaments during photopolymerization and validate a moving mesh computational fluid dynamics (CFD) model. The CFD model was used to develop an approach (predictive model) to accurately predict the final spreading coefficient of cured resin beads without the need for full numerical simulations. The predictive model combines the generalized theory of a Newtonian spreading filament with a characteristic viscosity μ_{ave} and time to gelation, τ_{gel}. Interestingly, μ_{ave} is shown to be a material parameter that does not depend on processing conditions, but only on the material's chemorheology. The predictive model is tested against a wide range of chemorheology and cure kinetic parameters and found to be in excellent agreement with the full numerical CFD simulations. This work will be very useful in estimating the final shape of beads during the material extrusion printing process, as well as a model to successfully parameterize extrusion-based 3D printers to control the shape of printed beads a-priori.

1. Introduction

Direct-Ink-Writing (DIW) is a state-of-art 3D material extrusion printing process that has high material compatibility, operational flexibility, low cost, ease of use, and the ability to print on non-planner substrates [1–4]. DIW involves the use of liquid inks, typically thermosetting resins, which gel/vitrify after deposition via a given reaction kinetics [1]. The method involves deposition of individual beads, either in the form of continuous filaments or discrete droplets, in a line-by-line, layer-by-layer fashion to create a complex three-dimensional part [1,3]. In addition to resin properties, the overall structure and mechanical properties of DIW printed parts are highly dependent on the shape and overlap of adjacent beads [1]. One major issue with DIW is that the uncontrolled spreading of the deposited beads before solidification make it difficult (if not impossible) to accurately vectorize 3D drawings such that part dimensions are precisely controlled in the printer [5,6]. Such lack of control leads to parts with poor fidelity, dimensional accuracy, and large inter-structure voids which diminish the mechanical integrity of the printed part [5,6]. Avoiding these issues, typically requires enormous resources via trial-and-error parameterization per resin, per printer. In this work, we develop a robust scaling approach and predictive model to estimate bead spreading of reactive resins for the purpose of DIW printer parameterization.

The spreading of beads in DIW is a complex process with several driving/resistive forces and time-dependent material parameters, such as rheology, caused by the polymerization reaction, i.e. the viscosity of the resin increases with polymerization [1,7–11]. The complexity and importance of time dependent material parameters on the spreading physics depends on the relative rates of spreading and reaction kinetics. Depending on the thermoset chemistry and reaction scheme, the polymerization reaction can be fast or slow compared to the spreading physics [7,8]. Spreading physics are a competition between driving and resistive forces. When a droplet/filament touches the substrate, the gradient in curvature (i.e. Laplace pressure) and gravity drive spreading, while fluid inertia and viscous dissipation resist spreading [12–14]. The balance between these forces dictates the rate of spreading and its timescale, τ_s.

The amount of the resin spreading depends on the reaction rate, i.e. kinetic timescale τ_k, compared to the spreading timescale, τ_s [7].

* Corresponding author.
E-mail address: nja49@drexel.edu (N.J. Alvarez).

https://doi.org/10.1016/j.addma.2024.104163
Received 19 January 2024; Received in revised form 22 March 2024; Accepted 23 April 2024
Available online 25 April 2024

For example, slow-curing resin systems, such as silicone at room temperature, will significantly spread before reaching gelation, since $\tau_k \gg \tau_s$ at room temperature. Note that thermoset resins are typically Newtonian fluids until they reach gelation, where they become viscoelastic solids. Thus, systems such as silicone at room temperature would follow a Newtonian spreading (i.e. constant viscosity) up to a steady state shape long before the reaction forms a viscoelastic network. The dynamic and steady state shape of such reacting systems can be readily predicted using a generalized spreading theory. More specifically, we showed that the shape of the bead can be predicted using master spreading curves via a viscous timescale defined as $\tau_\mu = \mu R_0/\sigma$ at a given Bond number, Bo, and steady advancing contact angle, θ_s [15,16]. On the other hand, some resins, e.g. methacrylates, epoxies, polyurethane, etc., have much faster reaction kinetics such that $\tau_k \approx \tau_s$. In such systems, the shape of the bead is a complicated function of time and processing parameters. In another special case, where $\tau_k \ll \tau_s$, the bead is frozen at the time of deposition and the shape of the bead simply depends on the deposition physics. However, due to the fast rates of spreading, this limit is almost never achieved in practice.

The more interesting case is when $\tau_k \approx \tau_s$, i.e. when both spreading and curing are happening simultaneously. However, modeling this case requires accurate chemorheological and kinetic models [8]. The rate of change of chemical conversion (α) depends on the type of polymerization reaction, e.g., autocatalytic, and the rate of mass transfer. For example, autocatalytic reaction models such as that of Kamal et al. [17] take into account power-law curing behavior at early time, and diffusion-limited mass transfer at later times. For resins that do not undergo autocatalyzation, the reaction rate is traditionally described by a single nth order model [18]. The relationship between viscosity and chemical conversion (a.k.a chemorheological model) typically relies on experimental data [19,20]. For the most part, chemorheological models are phenomenological and are determined by measuring the change of viscosity with conversion. For thermoresponsive resins, this is also measured as a function of temperature [20], and temperature effects are modeled by either Arrhenius or Williams–Landel–Ferry (WLF) equations [21]. For photo-cure resin systems, the viscosity predominately depends on power density and the effect of reaction latent heat on the viscosity is usually ignored. The effect of α on viscosity is typically modeled using an exponential function [19], or a power-law function, e.g. the modified Castro-Macosko model [20].

There are only a few examples of spreading models for reactive beads found in the literature [7,8,22,23], where all of them are focusing on the droplets and the spreading of filaments has not received any attention. For example, Yu et al. [23] numerically investigated the spreading and thermal curing behavior of a silicone droplet on a heated substrate using a volume of fluid (VOF) approach. The authors compare their model to steady state shapes of experimental droplets, which shows relatively good agreement. However, this result is expected since the authors use a static contact angle model at the three phase contact line. Unfortunately, the authors did not compare their model to dynamic data, which is necessary to determine if the physics are accurately predicting the evolution of spreading with time. There are two important assumptions in this model that limit the applicability and generalizability of the results: (1) a static contact angle was used to model the three phase contact line, and (2) their chemorheological model was limited to a viscosity versus time fit to experimental data with no general kinetic rate equation [23]. Similarly, Sivasankar et al. [7] used a moving mesh with constant contact angle to describe the three phase contact line dynamics, but did use a chemorheological model to account for explicit cure kinetics. However, the authors do not compare their dynamic droplet spreading model with any experimental data of a curing droplet, and therefore it is difficult to ascertain whether the model can accurately predict dynamic droplet shapes. We have recently shown, along with others, that the dynamic contact angle (DCA) boundary condition is necessary to accurately predict dynamic spreading, but not necessary to predict steady state shapes [8,16]. Thus, for chemorheological conditions where the viscosity is changing on the timescale of spreading, a dynamic contact angle must be employed. For example, Xie et al. [8] used a Phase-Field approach accounting for cure kinetics and the dynamic contact angle boundary condition. The authors demonstrated the model against experimental data of thermally cured silicone droplet. However, the agreement between model and experiment was not sufficient enough for accurate prediction of the dynamic and final droplet shape. This was most likely due to the poor agreement between the chemorheological model and experimental data. In general, the literature is focusing on the reactive droplets where does not appear to be any generalized solution or model to predict the spreading physics of a reactive resin.

In this work, we develop a general spreading model for photocurable droplets and filaments using experimental analysis and numerical simulation. The model is used to develop a predictive scaling approach to estimate the final shape of droplets and filaments when $\tau_s \approx \tau_k$. There are several differences that distinguish this work from the literature, namely, this work is interested in the spreading of cylindrical filaments for application in DIW printing, and focuses on a generalized solution to predict the spreading physics of a reactive resin. The organization of the paper is as follows. We first characterize the photo-cure kinetics and chemorheology of two different model resins. We then experimentally quantify the simultaneous spreading and curing of both filaments and droplets at different operating conditions. This data is compared to a full numerical model considering the dynamic spreading of photocurable droplets and filaments for model validation and demonstration of predictability. The model is validated using experimental cases where spreading and curing occur on similar timescales, i.e. $\tau_s \approx \tau_k$. Finally, we develop a predictive model to estimate the final shape of reactive beads without the use of fluid specific simulations. The results of our study offer avenues to successfully control the shape of printed beads via *a-priori* parameterization of the printing parameters.

Table 1
Measured and previously reported properties of DA-2 resin formulation [24].

Property	DA-2	Tenacious
Viscosity, μ [Pa s]	440 ± 50	410 ± 23
Surface tension, σ [mN/m]	35.1	31.8
Density, ρ [kg/m^3]	1105	1130
Static contact angle, θ_s [deg.]	19.6 ± 1.4	12.3 ± 0.3
Depth of penetration (@405 nm), D_p [μm]	550 ± 55	380 ± 55
Critical energy (@405 nm), E_C [mJ/cm^2]	5.6 ± 0.5	[–]

2. Materials and methods

2.1. Resin properties

Two well characterized photopolymerizable resins, i.e., DA-2 and Tenacious, were used for all experiments. DA-2 is composed of Bisphenol A glycerolate dimethacrylate (Bis-GMA 37.5 wt.%), ethoxylated bisphenol A dimethacrylate (Bis-EMA 37.5 wt.%), and 1,6-hexanediol dimethacrylate (HDDMA 25 wt.%) [24]. 0.7 wt.% phenylbis(2,4,6-trimethylbenzoyl)phosphine oxide (PPO, or bisacylphosphine oxides, BAPO) was dissolved into the DA-2 resin for use as a photoinitiator, purchased from MilliporeSigma (St. Louis, MO, USA). Tenacious is a commercial resin which is a mixture of Bisphenol A ethoxylate diacrylate and urethane acrylate and was purchased from Siraya tech (San Gabriel, CA, USA). Physical properties of photo-curable DA-2 and Tenacious resins are presented in Table 1:

2.2. Cure kinetics and chemorheology

The cure kinetics of DA-2 was previously measured using a real time photo-infrared technique operating in ATR mode (Nicolet™ 6700

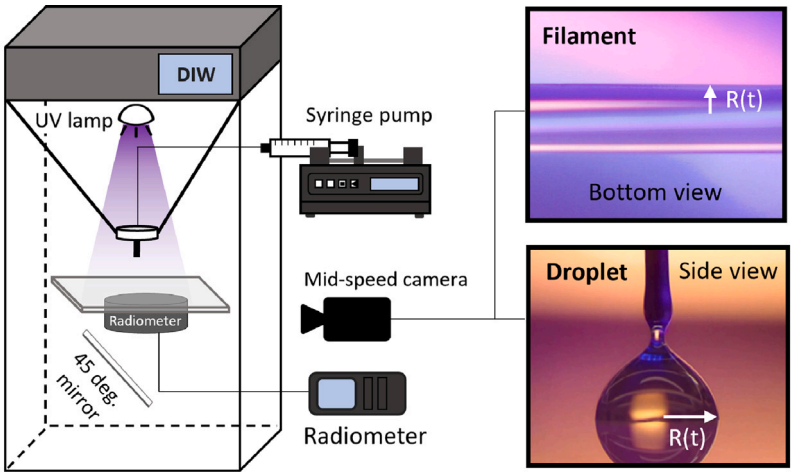

Fig. 1. A schematic of the experimental set-up used to quantify the deposition and spreading of filaments and droplets.

Table 2
Best-fit kinetic parameters for Eq. (1).

Parameters	α_u	n	k	ω
DA-2	0.74	4.4	0.3	0.71
Tenacious	1.06	2.71	0.05	0.71

FT-IR Spectrometer, Thermo Fisher Scientific, Waltham, MA, USA) and fit to a general multi-order reaction kinetic, Eq. (1) [25]. The photo-cure reaction kinetic of Tenacious was also measured using the same technique and fitted by Eq. (1). See Supplementary Information S1 for details of measurements, Fig. S1.

$$\alpha = \alpha_u - \left[\alpha_u^{(1-n)} - (1-n)kP^{\omega}(t-t_{oi})\right]^{\frac{1}{1-n}}, \quad (1)$$

where t is the irradiation time, t_{oi} is the oxygen inhibition time, P is the light power density in mW/cm^2, a_u, ω, k, and n are best fit model parameters given in Table 2. Note that $t_{oi} = E_{oi}/P$, where oxygen inhibition energy, E_{oi} = 4.61 and 2 mJ/cm^2, for DA-2 and Tenacious respectively.

The light power density, P, exponentially decays through the resins and in the light direction (z-axis). Using the Beer–Lambert law, $P(z)$ can be calculated (Eq. (2)).

$$P = P_0 exp(-z/D_p). \quad (2)$$

Chemorheology was measured using the DHR-3 Rheometer (Waters™/TA Instrument) equipped with photo-cure accessory. The sample was irradiated using 405 nm light through transparent parallel plates with a gap height of 150 μm to initiate the polymerization reaction while measuring the viscosity. The power density was measured at the surface of the parallel plates using a radiometer (ILT2400, International Light Technologies, Peabody, MA, USA). The viscosity as a function of time was measured using a shear rate of 1 1/s at different UV light power densities.

2.3. Quantification of bead spreading

We developed an in-situ device to measure the simultaneous spreading and curing of test resins in the form of droplet and continuous filament onto microscope glass slides (AmScope™). This set up includes a modified Delta Wasp 2040 Clay Printer to deposit the beads, a custom 45° flat mirror platform under the glass slide to reflect the bottom side of the beads, a mid-speed camera (HAYEAR, HY-2307, 2 M pixels with pixel size of 1.43×1.43 μm and 60 fps) with microscope zoom lens, and a precise syringe pump (HARVARD Apparatus, PHD 2000). A 405 nm lamp was used to irradiate the droplet and filament as shown in Fig. 1. The power density of the lamp was measured using the radiometer described above. The power density, P_0, of the lamp and initial size of the bead, R_0, were the only experimental variables. The power density ranged from 0.1 to 2 mW/cm^2 and was adjusted by the distance of the light source from the substrate. For droplets, R_0 was controlled via the needle diameter (25 and 27 Gauge needles with OD = 0.51 and 0.40 mm, respectively). For filaments, R_0 was controlled by the ratio of infill flow rate (Q = 45 mL/min) and nozzle velocity ($V_N \approx 70$ mm/s) using a mass balance, i.e. $R_0 = (Q/\pi V_N)^{0.5}$ [15]. Prior to each experiment, a new glass slide was washed with Isopropanol (VWR, CAS No. 67-63-0) and subsequently rinsed using DI water (18.2 MΩ· cm EMD Millipore Corporation). Each experiment was repeated at least 3 times to ensure reproducibility and the average values and standard deviation were reported. The basal radius, $R(t)$, was measured from underneath the spreading bead via the camera and was analyzed using a custom Matlab script.

2.4. Numerical modeling and simulation

The governing equations are the same presented in our previous work on the spreading of Newtonian droplets [16] and filaments [15]. However, in this study we couple the governing equations with cure kinetics and chemorheology. The Finite Element Method (FEM) model parameters were kept similar as before and the equations were solved using COMSOL multiphysics v.5.6. considering 2D-axisymmetric and 2D-symmetric frameworks for droplet and filament, respectively. The model geometry and corresponding mesh grids are shown in Fig. S3. We used the smallest mesh size criteria of $R_0/30$ to ensure the independence of the result to mesh grid spacing [15,16]. To keep the quality of the mesh above 0.1, a dynamic remeshing constraint was used to rebuild the entire mesh domain during the simulation. For completeness, the governing equations and boundary conditions are presented below:

Governing equations

To determine the distribution of the pressure p and velocity field ($\bar{u}$), Navier–Stokes (Eq. (3)) and continuity (Eq. (4)) were solved. However, the viscosity of the fluid, μ, is not constant and changes according to the chemorheology of the resin (Eq. (9)), which in turn depends on the cure kinetic (Eq. (1)). Furthermore, cure kinetic is an ODE which highly depends on the received light power density by the resin (Eq. (2)). Therefore, Eq. (2),(1), and (9), were coupled with the unsteady Navier–Stokes and continuity to fully model the process of simultaneous spreading and curing.

$$\rho\left(\frac{\partial \bar{u}}{\partial t} + \bar{u}\cdot\bar{\nabla}\bar{u}\right) = -\bar{\nabla}p + \mu(\alpha)\nabla^2\bar{u} + \rho\bar{g} \quad (3)$$

$$\nabla \cdot \bar{u} = 0. \tag{4}$$

Boundary conditions

At the bead–substrate interface, a Navier-slip boundary condition with no penetration were used (Eqs. (5) and (6)), where β is the slip length equal to 1/5×mesh size. Note that the Navier-slip relaxes the stress singularity at the interface, but does not significantly contribute to the bulk motion of fluid, i.e., spreading is insensitive to the magnitude of β [16]. The tangential and normal stress balance was used at the air–liquid interface (Eq. (7)) to track the position of the bead's free surface, S, over time. At the triple line, i.e., the bead–substrate–air interface, an empirical dynamic contact angle model (Eq. (8)) was applied, which relates the dynamic contact angle to the contact line velocity via capillary number, Ca. We have previously validated Eq. (8) for both cylindrical filaments and spherical droplets [15,16].

$$\bar{\tau}_f = \mu(\alpha)\frac{\bar{u}}{\beta} \tag{5}$$

$$\bar{u} \cdot \bar{n}_{wall} = 0 \tag{6}$$

$$\bar{n} \cdot (\bar{\bar{T}}^I - \bar{\bar{T}}^{II}) = \sigma(\bar{\nabla} \cdot \bar{n})\bar{n} - \bar{\nabla}\sigma \tag{7}$$

$$\frac{cos(\theta_s) - cos(\theta_D)}{cos(\theta_s) + 1} = tanh(A\mathrm{Ca}^B), \tag{8}$$

where $\bar{\bar{T}}$ is the total stress, i.e., $p\bar{\bar{I}} - \bar{\bar{\tau}}$, and the RHS of Eq. (7) represents the force per unit area due to surface tension, σ. θ_D is the dynamic contact angle. $\mathrm{Ca} = \mu\bar{u}/\sigma$ is the Capillary number. A and B are fitting parameters equal to 7.32 and 0.702, respectively. More details are given in Ref. [16].

3. Results and discussion

Since the numerical simulations are concerned primarily with the change in shape of the bead (droplet/filament) during spreading, the results will be discussed in terms of $R(t)$, the basal radius. It should be noted that the final shape of non-curing bead is limited by the equilibrium contact angle (balance of interfacial energies) [13]. However, for a bead undergoing chemical reaction, the polymerization process increases viscosity and ultimately arrests the shape at a contact angle above or equal to the steady state contact angle. Recall that the degree of spreading during the polymerization process depends on the balance of timescales, i.e. τ_s to τ_k. Two scenarios are considered: **(i)** a slow-curing system, i.e. $\tau_s \ll \tau_k$, and **(ii)** a fast curing system, i.e. $\tau_s \approx \tau_k$.

3.1. Slow-curing systems with $\tau_s \ll \tau_k$

For the case of $\tau_s \ll \tau_k$, the curing process occurs after significant spreading of the bead. In other words, the spreading process is essentially governed by the initial properties of the printing material. For this case, we previously modeled the spreading dynamics for both droplet and filament considering a fluid with constant properties [15,16]. We showed that at a given Bo and θ_s, the scaled basal radius, referred to as the spreading coefficient, $R(t)/R_0$, is a unique function of the scaled spreading time, t/τ_μ, where τ_μ is the viscous timescale. Fig. 2 shows the spreading coefficient for droplets and filaments at $\theta_s = 20°$ corresponding to the spreading of DA-2 resin on glass slide (see Table 1) at different Bo. Figure S4 also shows the master curves corresponding to Tenacious-glass slide $\theta_s = 12°$. The dynamic shape of a spreading bead, either droplet or filament, can be readily determined using these master curves and properties of the fluid, i.e., density, viscosity and its initial size. Similar master spreading curves at different θ_s for both droplets and filaments can also be found in our previous works [15,16].

3.2. Fast-curing systems with $\tau_s \approx \tau_k$

For the case of $\tau_s \sim \tau_k$, more common in DIW processes, there is simultaneous spreading and curing of the bead that ultimately dictates the final bead shape. Polymerization increases the viscosity of the resin, slowing down the spreading process. This results in smaller spreading coefficients and larger apparent contact angles at long times [8]. Although polymerization also affects surface tension and density, the changes are very small, i.e. less than 10 percent [24] and therefore are ignored. The following sections are organized as follows. First we characterize the chemorheology of the model resin for use in the numerical model. Followed by experimental model validation using curing spreading drops and filaments. Finally, we demonstrate a general method of predicting final cured bead shape without the use of fluid specific simulations.

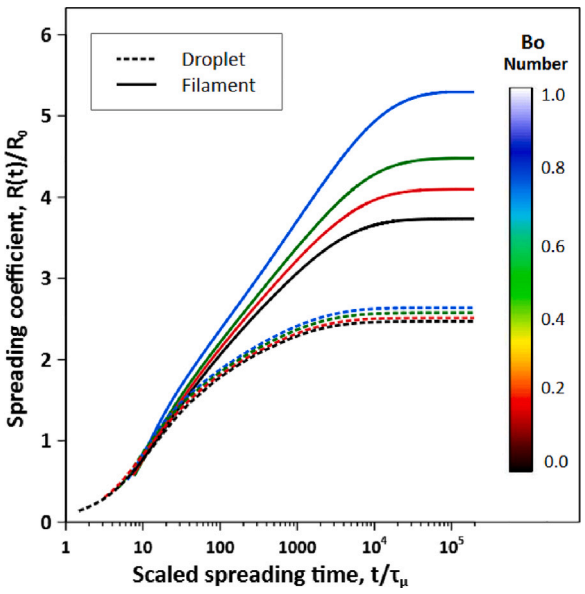

Fig. 2. Newtonian master curves for both droplet (dotted lines) and filament (solid lines) at $\theta_s = 20°$. More details are given in Ref. [15,16].

3.2.1. Chemorheology model

The inset of Fig. 3 shows the chemorheology data for DA-2 resin measured at average power densities of P_{ave} = 1, 2, and 4 mW/cm^2. See Supplementary Information S3 for the average power density calculation. As power density increases, the viscosity increases faster with time. The dependence on time can be eliminated by converting time to α using Eq. (1), such that a chemorheological master curve is determined. Fig. 3 shows the chemorheological master curve for DA-2. Several models exist in the literature to empirically fit chemorheological data. For example, there are models based on gel point physics, see Castro and Macosko [26], and exponential based models [19,27]. Note that both of these chemorheological models were implemented in the spreading model development. We found that the gel point models consistently under predicted the spreading of the interfaces. This seems to be due to the fact that in these models the viscosity diverges at the gel point, freezing the shape at early times. However, the experimental data shows that the viscosity is a continuous function of conversion. Therefore, the data was fit to an exponential chemorheological model, reported in [19,27], given by

$$\mu = \mu_0 exp(\gamma + \kappa\alpha), \tag{9}$$

where μ_0, γ, and κ are fitting parameters. The chemorheological data for Tenacious can be found in Fig. S2. Table 3 shows the best-fit values of model parameter for both DA-2 and Tenacious test resins. Note that γ contains the activation energy of the viscous flow and is a function of reaction temperature for thermally curable resins [19]. However, for photocurable systems, the effect of temperature can be ignored and γ is almost constant. Therefore, μ_0 and γ are dependent parameters with

Table 3
Best-fit chemorheological parameters for Eq. (9).

Parameters	μ_0	γ	κ
DA-2	0.1	1.48	40
Tenacious	0.1	1.41	60

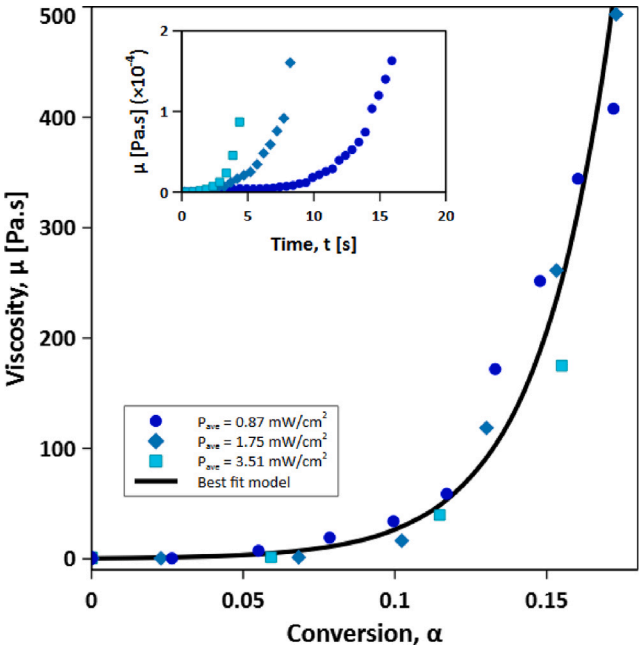

Fig. 3. Chemorheology of DA-2 resin under various irradiation intensities at 25 °C. Inset: measured cure viscosity over time.

$\mu_0 exp(\gamma) = 0.44$ and 0.41 Pa s, equal to the initial viscosity of the DA-2 and Tenacious, respectively. The best-fit model is shown via a solid line in Fig. 3.

3.2.2. Numerical model validation

Experimental spreading data for DA-2 droplets and filaments at two different light power densities are compared to numerical model predictions in Fig. 4. Similar model validation data for Tenacious droplet is shown in Fig. S5. The results show good agreement between model predictions and dynamic spreading and final shape with a maximum calculated relative error < 10%. Thus, the numerical model presented here incorporates all the necessary physics to accurately predict the shape dynamics of curing beads. However, the model parameters are very specific to the spreading fluid, and thus would require new parameterization and full numerical simulations for each system. Although possible, this is quite experimentally and computationally expensive. In the following section, we propose a simple general model to accurately predict the spreading behavior of curing droplets/filaments without the need for full numerical simulations.

3.2.3. Predictive model

Recall that the master curves in Fig. 2 allow for the prediction of a droplet/filament shape at any time during the spreading process of a non-curing Newtonian fluid. Unfortunately, such master curves are not possible for curing systems as the shape depends strongly on the reaction kinetics and transient viscosity. However, we discovered that the spreading dynamics of a curing bead can be predicted using Fig. 2 by considering a characteristic viscosity, μ_{ave} and a timescale for gelation, τ_{gel}. We postulate that the shape of the bead stops changing at the gel point, i.e. $\alpha = \alpha_{gel}$. Therefore, the spreading time t_s, would be equal to the gel time $\tau_{gel} = f(\alpha_{gel}, P)$, which is determined from the cure kinetic model for a given power density using Eq. (1).

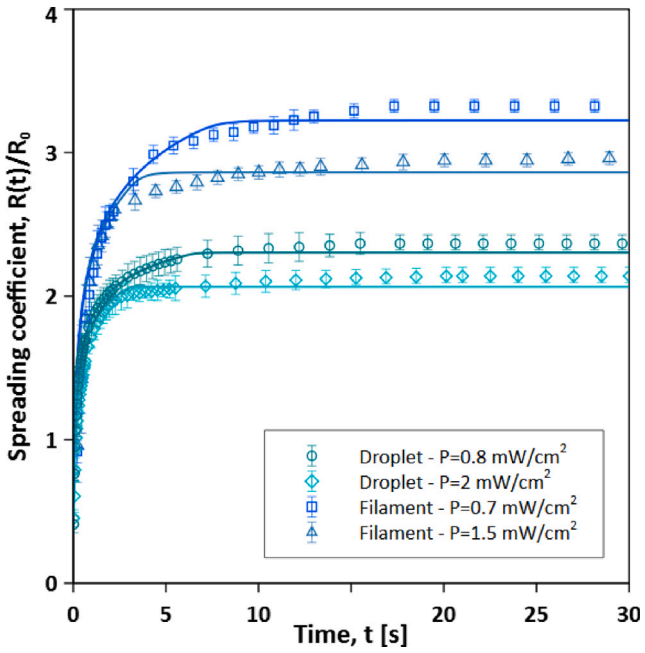

Fig. 4. Experimental data (dots) vs simulation (lines) for both DA-2 droplet and filament in terms of evolution of spreading coefficient over time at different light power densities.

One obvious selection for the characteristic viscosity is the time averaged viscosity during the curing process. A simple test of this hypothesis is to determine the characteristic viscosity using Fig. 2 at different power densities, since the time averaged viscosity would have a strong dependence on the power density. We did full numerical simulations of DA-2 filament spreading at different power densities to determine the final basal radius, R_F, and calculate R_F/R_0. The Newtonian master curves, Fig. 2, were used to determine the corresponding scaled spreading time, i.e. t_s/τ_μ, where $t_s = \tau_{gel}$ to achieve R_F/R_0, and the characteristic viscosity was determined using $\mu_{ave} = \tau_{gel}\sigma/R_0$. Surprisingly, Fig. 5a shows that the μ_{ave} is independent of the power density for all numerical experiments. This clearly shows that the resulting characteristic viscosity is a material parameter, and therefore does not depend on processing conditions, e.g., power density. In other words, a time averaged viscosity is *NOT* appropriate to describe the characteristic viscosity, since the time average viscosity clearly depends on the power density.

The lack of dependence of the characteristic viscosity on power density suggests that the relationship between viscosity and conversion dictates the spreading physics. In other words, how fast viscosity changes, i.e. $d\mu/dt$, compared to the rate of curing reaction, i.e. $d\alpha/dt$, govern the spreading, which is defined as $d\mu/d\alpha$. We argue that the early conversion dependence of μ plays a larger role in the final shape, as the shape of a bead changes predominately in the early stage of spreading. Therefore, considering the $\frac{d\mu}{d\alpha} = \frac{d\mu}{d\alpha}\Big|_{\alpha=\alpha_0}$ and integrating up to the gel point, we can have a new definition for characteristic viscosity, called $\mu_{asymptotic}$, given by

$$\mu_{asymptotic} = \mu_i + \frac{d\mu}{d\alpha}\Big|_{\alpha=\alpha_0}(\alpha_{gel} - \alpha_0), \tag{10}$$

where μ_i is the initial viscosity of resin. See Supplementary Information S6 for detailed calculations. Fig. 5b depicts the definition of $\mu_{asymptotic}$ using the chemorheology model for DA-2. $\mu_{asymptotic}$ is defined as the intersection of a tangent line at small conversion and the vertical line corresponding to the gelation point, α_{gel}. Using this method, $\mu_{asymptotic}$=3.08 Pa s for DA-2, which is shown as a solid line in Fig. 5a

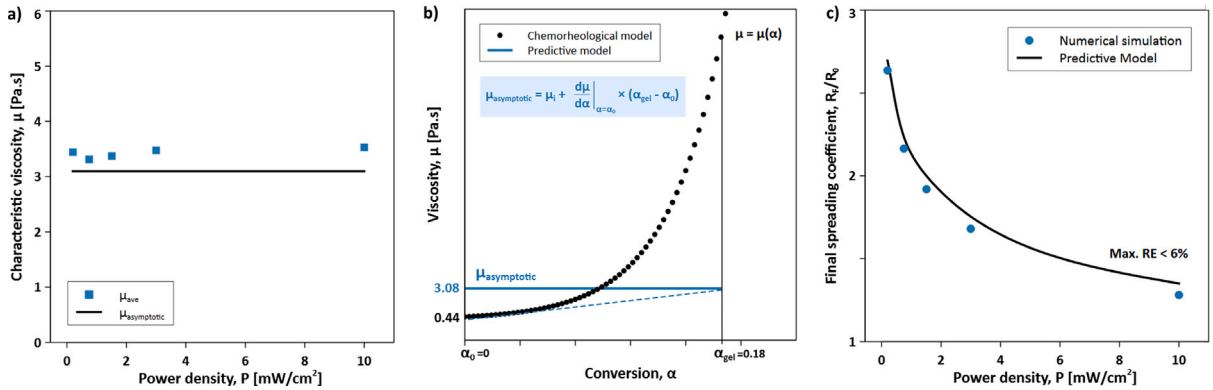

Fig. 5. **(a)** μ_{ave} vs $\mu_{asymptotic}$ for DA-2 filament spreading, **(b)** Calculation procedure of $\mu_{asymptotic}$ using the chemorheological model, **(c)** Final spreading coefficient of the DA-2 filament predicted by numerical simulation vs. predictive model. Note, the initial size of the filament $R_0 = 0.34$ mm was used in all simulations. We also assumed no oxygen inhibition, i.e., $t_{oi} = 0$ for the data presented here.

and showing excellent agreement with the numerically determined μ_{ave}.

With τ_{gel}, $\mu_{asymptotic}$, and Fig. 2 we have all the necessary information to make predictions on the spreading shape of curing filaments/droplets. The first step is to calculate the scaled spreading time τ_{gel}/τ_{μ}, where $\tau_{\mu} = \mu_{asymptotic} R_0/\sigma$. The second step is to calculate the $\text{Bo} = (\Delta\rho R_0^2\, g)/\sigma$. The last step is to determine the $R(\tau_{gel}/\tau_{\mu})/R_0$ for the given Bo and θ_s, which corresponds to the predicted final spreading coefficient. Fig. 5c shows the comparison of the predicted final spreading coefficient for DA-2 filaments compared to full numerical simulations. As observed, there is excellent agreement between the prediction and the numerical simulation. The prediction always slightly overpredicts the spreading shape by a maximum error less than 6%. Note that the predictive model cannot be used to predict the shape at intermediate times, only the final shape at times longer than the gel time. However, for DIW printing, we are only concerned with the final bead shape.

The same result was obtained for the prediction of the spreading coefficient for DA-2 curing droplets considering a wide range of power densities, see Supplementary Information S7. Overall, the predictive model can be successfully used to estimate the final shape of both curing droplets and filaments.

While the results above are only for a single chemorheological parameter set, we tested a range of chemorheological model parameters to determine whether the $\mu_{asymptotic}$ concept is generalizable. A series of μ_0s were chosen to drastically change the range of $\mu_{asymptotic}$ via Eq. (10). Note that a change in μ_0 results in a change of both the intercept and the slope in Eq. (10). Fig. 6a shows the different chemorheological models tested. Fig. 6b shows excellent agreement between the μ_{ave} and the predicted $\mu_{asymptotic}$ from Eq. (10), which translates to excellent agreement between the full numerical final spreading coefficient and the predicted final spreading coefficient. Overall, the predictive model is able to capture the final spreading coefficient for different Chemorheological models with a maximum relative error of less than 4% for all cases. This model should prove very useful in predicting the final shape of curing droplets and filaments in the DIW printing process.

3.2.4. Effect of oxygen inhibition

The simulations and data analysis above does not consider the effect of oxygen inhibition on the spreading physics. However, in most of practical cases, especially for free radical photo-polymerization mechanisms, there is a delay period with no polymerization due to oxygen inhibition [25]. The oxygen inhibition time period, τ_{oi}, is a resin property which depends on the amount of O_2 in the resin system. For all of the photo-cure resin systems, the τ_{oi} is inversely proportional to the power density. Higher power density increases the rate of the photo-initiator free-radical reaction which results in faster consumption of O_2 in the system. Fig. 7 shows schematic representation of a filament spreading and its corresponding viscosity evolution in the presence of oxygen inhibition. When the filament touches the substrate, it starts to spread like a Newtonian resin as its properties are constant due to the oxygen inhibition, see blue shadowed region in Fig. 7. After $t = \tau_{oi}$, the viscosity increases due to the polymerization reaction and slows down the spreading, see red shadowed region in Fig. 7. In the previous section, we showed that the shape of the filament in the absence of oxygen inhibition (spreading with no delayed curing) can be predicted using a constant viscosity, $\mu_{asymptotic}$ (predictive model). Now we modify the predictive model to incorporate the effect of oxygen inhibition. As explained above, during the oxygen inhibition period, the resin viscosity is constant and equal to its initial value. Therefore, we can define two dimensionless times, one for the oxygen inhibition regime and one for the curing regime. Since the spreading occurs on a single master curve given Bo and θ_s, then we expect that the overall dimensionless spreading time to be a sum of these individual contributions. More specifically, the dimensionless spreading time is split into a contribution from the oxygen inhibition, $\tau_{oi}/\tau_{\mu,oi}$, and a contribution from the curing, $(\tau_{gel} - \tau_{oi})/\tau_{\mu,cure}$, such that

$$\frac{t}{\tau_{\mu}} = \frac{\tau_{oi}}{\tau_{\mu,oi}} + \frac{\tau_{gel} - \tau_{oi}}{\tau_{\mu,cure}}, \tag{11}$$

where $\tau_{\mu,oi} = \mu_0 R_0/\sigma$ is the viscous timescale for the oxygen inhibition regime, and $\tau_{\mu,cure} = \mu_{asymptotic} R_0/\sigma$ is the viscous timescale for the curing regime. Note that in chemorheological models with explicit oxygen inhibition, the τ_{gel} calculated includes τ_{oi}, which explains the need for the $\tau_{gel} - \tau_{oi}$ term.

Fig. 8 shows a comparison of the final spreading coefficient for the numerical experiments compared to the predictions using the dimensionless time defined by Eq. (11) (black dotted line) for a wide range of oxygen inhibition times and cure times represented by a ratio, $\tau_{oi}/\tau_{\mu,cure}$. The black curve shows excellent agreement with the final spreading coefficient demonstrating that Eq. (11) is capable of taking into account the cure and oxygen inhibition contributions to the overall spreading. Fig. 8 also shows the individual predictions of the final shape for each regime: spreading due to oxygen inhibition only (blue) and spreading during cure only (red line). At low ratios, i.e. negligible oxygen inhibition, the red line prediction is in good agreement with the filament shape, as discussed in the previous section. However, the red line under-predicts the shape at high ratios when the oxygen inhibition becomes dominant. Inversely, at high ratios, i.e. relatively long oxygen inhibition, the blue line prediction is in good agreement with the filament shape. For intermediate ratios, the sum of these two lines (black dashed line) predict the overall shape. These results show that Eq. (11) can successfully predict the shape of a curing bead in the presence of oxygen inhibition. In fact, Eq. (11) is the proper

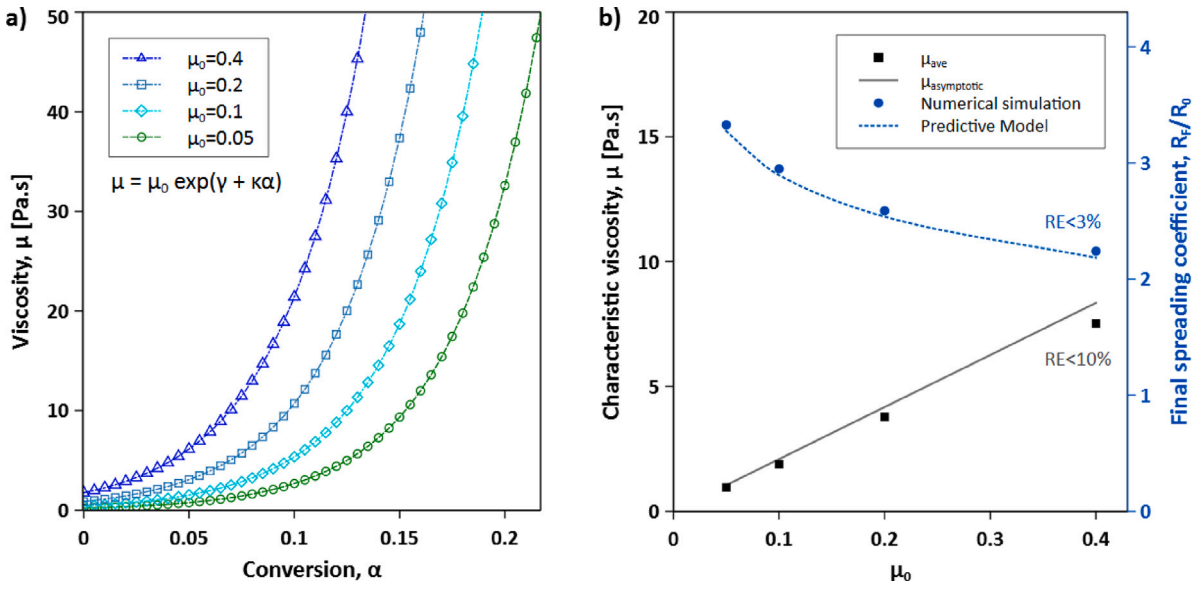

Fig. 6. **(a)** Chemorheological models with different μ_0 and constant $\gamma = 1.48$ and $\kappa = 25$, **(b)** μ_{ave} vs $\mu_{asymptotic}$ (black dots) and numerical simulation vs predictive model (blue dots) corresponding to the chemorheological models. Note, numerical simulations were done at $P = 0.2$ mW/cm^2 and $R_0 = 0.34$ mm. Other resin properties were the same as DA-2.

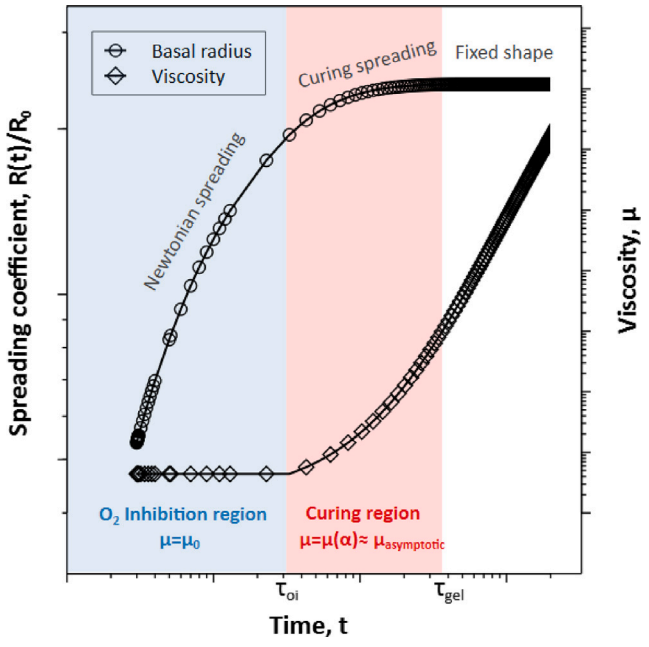

Fig. 7. Schematic representation of the effect of O_2 inhibition on the spreading of a curing bead.

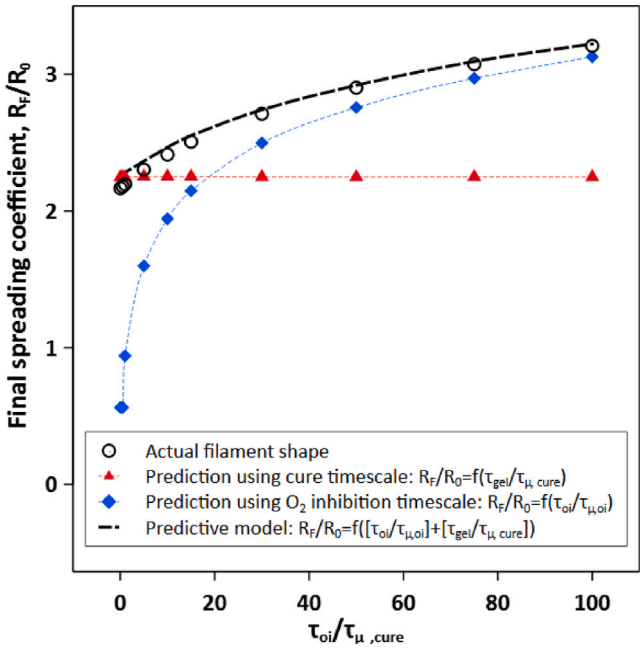

Fig. 8. Prediction of final spreading coefficient using the modified predictive model to include the effect of oxygen inhibition.

dimensionless time to use for all chemorheological models since it captures all necessary physics.

To further validate our predictive model including oxygen inhibition, we used Eq. (11) to predict the experimentally measured final shape of Tenacious resin droplets. The final spreading coefficients of Tenacious were experimentally measured using a 0.96 mm droplet under UV illuminations of 0.14 and 0.26 mW/cm^2. The experimental data is shown in Table 4.

The predictive model requires as an input the scaled overall spreading time given by Eq. (11). $\mu_{asymptotic} = 4.1$ [Pa s], $\tau_{\mu,oi} = 0.012$ [s], and $\tau_{\mu,cure} = 0.122$ were calculated using Eq. (10), and material properties listed in Table 1. τ_{oi} and τ_{gel} were determined from Eq. (1) using $\alpha_{gel} = 0.15$. Given the scaled overall spreading time t/τ_μ and Bo, the final spreading coefficients R_F/R_0 were predicted using the corresponding Newtonian master curves, see Fig. S4. Table 4 shows all calculated parameters used to predict the spreading of Tenacious droplets for two power densities, and a comparison of the predicted and experimentally measured R_F/R_0. It can be clearly seen that the predictive model shows excellent agreement with the final spreading coefficient of tenacious resin with relative error less than 5%. This additional experimental data shows that the predictive model works for different photo-curing resins, as well as different degrees of oxygen inhibition.

3.2.5. Practical uses of the predictive model

One of the practical aspects of this novel predictive model is the ability of achieving a specific shape of the printed bead by controlling process parameters of power density and R_0. The predictive model

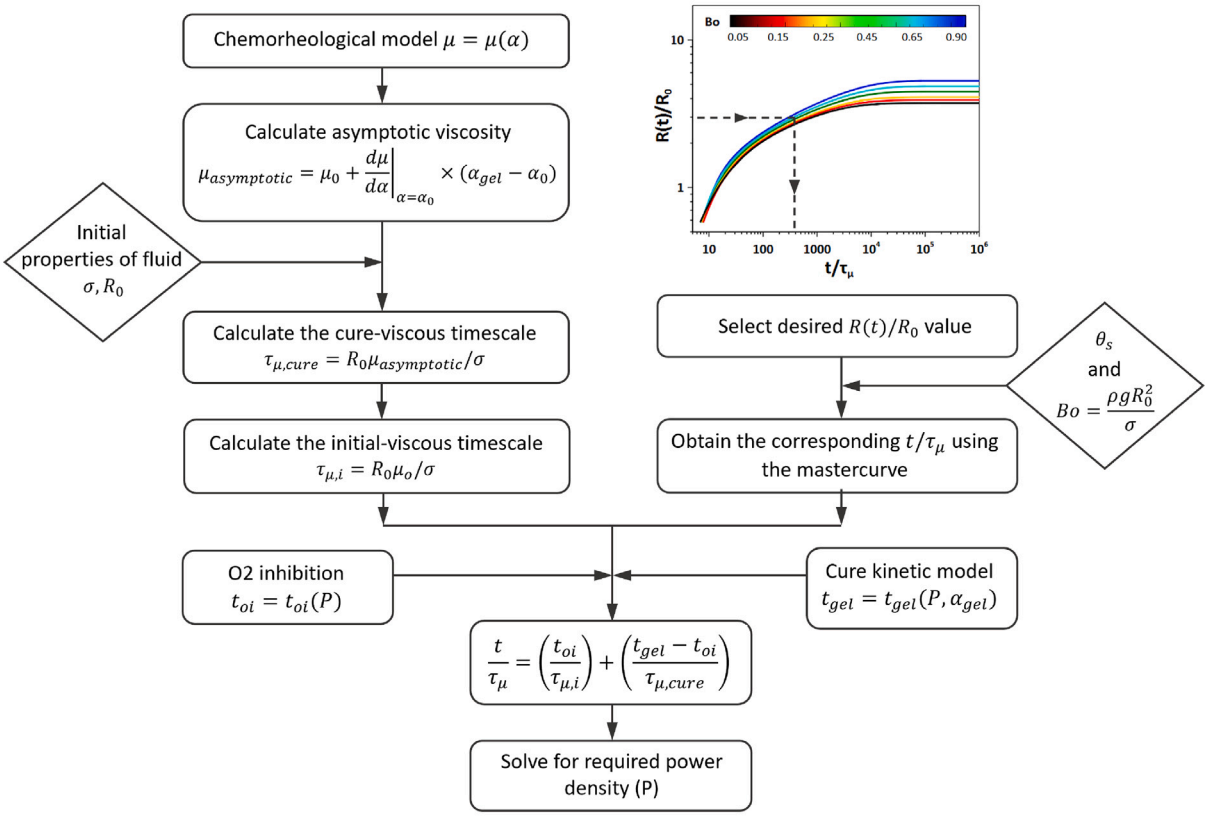

Fig. 9. Calculation procedure of proposed predictive model to estimate the required power density for a desired bead shape.

Table 4
Calculated parameters used to estimate the spreading coefficient of Tenacious droplet at different power densities along with experimental data measured at the reported power densities. The experimental data represents the average of three experimental points and their standard deviation.

P [mW/cm^2]	τ_{oi} [s]	τ_{gel} [s]	t/τ_μ	R_F/R_0	R_F/R_0 experimental
0.14	14.28	12.74	1253.15	2.51	2.55 ± 0.05
0.26	7.69	8.17	692.56	2.37	2.46 ± 0.08

described above relates the power density to the shape of the bead, and therefore estimates the required power density to achieve a final bead shape. Fig. 9 shows a flowchart detailing the method of calculating the power density required for a desired shape. Given a desired scaled spreading coefficient R_F/R_0, the Newtonian spreading master curves are used to determine the value of t/τ_μ required. The flowchart requires as inputs the chemorheological and kinetic properties of the resin, i.e. conversion versus time and viscosity versus conversion. These relationships give μ_0, $\mu_{asymptotic}$ using Eq. (10), and τ_{oi} and τ_{gel} as a function of power density. These values are then coupled with Eq. (11) to determine the power density required to achieve the necessary dimensionless spreading time.

4. Conclusion

This work presents the first numerical CFD model that captures the appropriate physics for the dynamic spreading of resin beads (droplets and filaments) during photo-polymerization. The numerical model was validated using experimental results and used to develop a simple approach to predicting the final shape (predictive model) of cured beads using the general theory of Newtonian spreading. The predictive model does not require any computational fluid dynamics, but rather uses Newtonian spreading master curves to accurately predict the final shape of a curing bead using a characteristic viscosity μ_{ave} and a timescale for gelation, τ_{gel}. In other words, we showed that a curing bead and a Newtonian bead with a constant viscosity of μ_{ave} achieve the same spreading coefficient when $t = \tau_{gel}$, where μ_{ave} and τ_{gel} are determined from a simple analysis of the fluid's chemorheology and cure kinetics, respectively. Moreover, the model is capable of predicting the shape of curing beads with and without oxygen inhibition. The applicability of the predictive model was successfully tested against a range of chemorheological parameters and process parameters and found to be in excellent agreement with the full numerical simulations. These results and the predictive model approach will be an invaluable tool for DIW 3D printing applications as a method of estimating the shape of the beads deposited on the build platform. Furthermore, we demonstrate how the model can be used to determine the appropriate process parameters to achieve a specific bead shape. This should significantly reduce the trial-and-error approach and limit the printing window to a tractable, relevant space. In addition, we expect that this model can be incorporated into 3D printing vectorization software to take into account the final bead shape when determining the line width and the layer height of each deposited bead. The extension of these concepts to the spreading of thermally curable resin systems is the subject of ongoing research.

CRediT authorship contribution statement

Amir Azimi Yancheshme: Writing – original draft, Visualization, Validation, Software, Methodology, Conceptualization. **Heedong Yoon:** Writing – review & editing, Methodology, Conceptualization. **Giuseppe R. Palmese:** Writing – review & editing, Funding acquisition, Conceptualization. **Nicolas J. Alvarez:** Writing – review & editing, Supervision, Methodology, Funding acquisition, Conceptualization.

Declaration of competing interest

The authors declare the following financial interests/personal relationships which may be considered as potential competing interests: Nicolas J. Alvarez reports financial support was provided by Army research laboratory. If there are other authors, they declare that they have no known competing financial interests or personal relationships that could have appeared to influence the work reported in this paper.

Data availability

Data will be made available on request.

Acknowledgments

Research was sponsored by the Army Research Laboratory, USA and was accomplished under Cooperative Agreement Number W911NF-17-2-0227. The views and conclusions contained in this document are those of the authors and should not be interpreted as representing the official policies, either expressed or implied, of the Army Research Laboratory or the U.S. Government. The U.S. Government is authorized to reproduce and distribute reprints for Government purposes not withstanding any copyright notation herein. NJA was also supported by the National Science Foundation, USA under grant no. CBET-1847140.

Appendix A. Supplementary data

The following files are available free of charge.

- Supporting information: supporting results and additional model details and derivations.

Supplementary material related to this article can be found online at https://doi.org/10.1016/j.addma.2024.104163.

References

[1] B. Mueller, Additive manufacturing technologies–rapid prototyping to direct digital manufacturing, Assem. Autom. (2012).
[2] B.G. Compton, J.A. Lewis, 3D-printing of lightweight cellular composites, Adv. Mater. 26 (34) (2014) 5930–5935.
[3] D.A. Rau, M.J. Bortner, C.B. Williams, A rheology roadmap for evaluating the printability of material extrusion inks, Addit. Manuf. 75 (2023) 103745.
[4] P. Wei, C. Cipriani, C.-M. Hsieh, K. Kamani, S. Rogers, E. Pentzer, Go with the flow: Rheological requirements for direct ink write printability, J. Appl. Phys. 134 (10) (2023).
[5] Y. Jin, D. Zhao, Y. Huang, Study of extrudability and standoff distance effect during nanoclay-enabled direct printing, Bio-Des. Manuf. 1 (2018) 123–134.
[6] S. Jang, A. Boddorff, D.J. Jang, J. Lloyd, K. Wagner, N. Thadhani, B. Brettmann, Effect of material extrusion process parameters on filament geometry and inter-filament voids in as-fabricated high solids loaded polymer composites, Addit. Manuf. 47 (2021) 102313.
[7] V.S. Sivasankar, H.S. Sachar, S. Sinha, D.R. Hines, S. Das, 3D printed micro-droplet curing: Unravelling the physics of on-spot photopolymerization, ACS Appl. Polym. Mater. 2 (2) (2020) 966–976.
[8] J. Xie, R. Randolph, G. Simmons, M. Vinciguerra, S. Suri, N. Bonini, A. Root, P.V. Hull, A.D. Mazzeo, Spreading of fast-curing, thermosetting silicones, Appl. Phys. Lett. 115 (25) (2019) 253701.
[9] J.A. Lewis, Direct ink writing of 3D functional materials, Adv. Funct. Mater. 16 (17) (2006) 2193–2204.
[10] L. Li, Q. Lin, M. Tang, A.J. Duncan, C. Ke, Advanced polymer designs for direct-ink-write 3D printing, Chem. Eur. J. 25 (46) (2019) 10768–10781.
[11] M. Layani, X. Wang, S. Magdassi, Novel materials for 3D printing by photopolymerization, Adv. Mater. 30 (41) (2018) 1706344.
[12] A.-L. Biance, C. Clanet, D. Quéré, First steps in the spreading of a liquid droplet, Phys. Rev. E 69 (1) (2004) 016301.
[13] A. Eddi, K.G. Winkels, J.H. Snoeijer, Short time dynamics of viscous drop spreading, Phys. Fluids 25 (1) (2013) 013102.
[14] K.G. Winkels, J.H. Weijs, A. Eddi, J.H. Snoeijer, Initial spreading of low-viscosity drops on partially wetting surfaces, Phys. Rev. E 85 (5) (2012) 055301.
[15] A. Azimi Yancheshme, G.R. Palmese, N.J. Alvarez, Predicting the dynamics and steady-state shape of cylindrical Newtonian filaments on solid substrates, Langmuir 39 (30) (2023) 10495–10503.
[16] A.A. Yancheshme, G.R. Palmese, N.J. Alvarez, A generalized scaling theory for spontaneous spreading of Newtonian fluids on solid substrates, J. Colloid Interface Sci. (2023).
[17] M. Kamal, S. Sourour, Kinetics and thermal characterization of thermoset cure, Polym. Eng. Sci. 13 (1) (1973) 59–64.
[18] P. Hubert, A. Johnston, A. Poursartip, K. Nelson, Cure kinetics and viscosity models for hexcel 8552 epoxy resin, in: International SAMPE Symposium and Exhibition, SAMPE; 1999, 2001, pp. 2341–2354.
[19] C.-L. Lee, K.-H. Wei, Curing kinetics and viscosity change of a two-part epoxy resin during mold filling in resin-transfer molding process, J. Appl. Polym. Sci. 77 (10) (2000) 2139–2148.
[20] M. Ivankovic, L. Incarnato, J.M. Kenny, L. Nicolais, Curing kinetics and chemorheology of epoxy/anhydride system, J. Appl. Polym. Sci. 90 (11) (2003) 3012–3019.
[21] M.L. Williams, R.F. Landel, J.D. Ferry, The temperature dependence of relaxation mechanisms in amorphous polymers and other glass-forming liquids, J. Am. Chem. Soc. 77 (14) (1955) 3701–3707.
[22] R. De Ruiter, L. Royon, J.H. Snoeijer, P. Brunet, Drop spreading and gelation of thermoresponsive polymers, Soft Matter 14 (16) (2018) 3096–3104.
[23] X. Yu, R. Hu, L. Zhou, H. Wu, X. Luo, Spreading and curing behaviors of a thermosetting droplet- silicone on a heated surface, J. Harbin Inst. Technol. (New Series) 26 (4) (2019) 1–8.
[24] J. Tu, K. Makarian, N.J. Alvarez, G.R. Palmese, Formulation of a model resin system for benchmarking processing-property relationships in high-performance photo 3D printing applications, Materials 13 (18) (2020) 4109.
[25] J. Tu, Y. Kashcooli, N.J. Alvarez, G.R. Palmese, A practical framework for predicting conversion profiles in vat photopolymerizations, Addit. Manuf. 59 (2022) 103102.
[26] J. Castro, C. Macosko, Studies of mold filling and curing in the reaction injection molding process, AIChE J. 28 (2) (1982) 250–260.
[27] P.J. Halley, M.E. Mackay, Chemorheology of thermosets—an overview, Polym. Eng. Sci. 36 (5) (1996) 593–609.